BAYES' THEOREM AND EARLY SOLAR SHORT-LIVED RADIONUCLIDES: THE CASE FOR AN UNEXCEPTIONAL ORIGIN FOR THE SOLAR SYSTEM

EDWARD D. YOUNG

Department of Earth, Planetary, and Space Sciences, University of California Los Angeles, 595 Charles E. Young Drive East, Geology Building, Los Angeles, CA 90095-1567, USA; eyoung@epss.ucla.edu

ABSTRACT

The presence of excesses of short-lived radionuclides in the early solar system evidenced in meteorites has been taken as testament to close encounters with exotic nucleosynthetic sources, including supernovae or AGB stars. An analysis of the likelihoods associated with different sources of these extinct nuclides in the early solar system indicates that, rather than being exotic, their abundances were typical of star-forming regions like those observed today in the Galaxy. The radiochemistry of the early solar system is therefore unexceptional, being the consequence of extensive averaging of solids from molecular clouds.

Key words: astrochemistry – ISM: supernova remnants – meteorites, meteors, meteoroids – stars: Wolf–Rayet

1. INTRODUCTION

The conventional view of the origin of our solar system has been that the abundances of the radionuclides, especially the short-lived radionuclides (SLRs) with mean lives of several million years or less, are testament to close encounters with particular, often exotic, nucleosynthetic sources, including collapse supernovae (SNe) or asymptotic giant branch (AGB) stars (Cameran & Truran 1977; Wasserburg et al. 1996, 2006; Lugaro et al. 2014). Indeed, apparent excesses in SLRs have even been used as evidence for a supernova trigger for the formation of the solar system, an idea that has waxed and waned but persists still (Cameran & Truran 1977; Gounelle & Meynet 2012). Here it is shown that the initial abundances of the SLRs in the early solar system are likely typical of star-forming regions (SFRs) rather than exotic. This result stands in contrast to the notion that the solar system SLRs were overabundant relative to normal molecular cloud material and instead indicates that the radiochemistry of the early solar system is typical of massive SFRs like those observed today in the Galaxy; a comprehensive theory for the radiochemistry of the solar system is best cast in terms of a statistical analysis of SFR material rather than close encounters with a finite number of individual nucleosynthetic sources. The success of this approach in explaining the relative abundances of solar system radionuclides places the origin of the solar system squarely in the realm of business as usual for SFRs and suggests that the abundances of individual nuclides should not be taken as evidence for individual stellar sources.

Theories for the provenance of the solar system radio-nuclides can be divided into two types of scenario. In the first type of scenario, the radiochemistry of the solar system has no significance beyond chance encounters between pre-solar materials and a variety of nucleosynthetic sources (Wasserburg et al. 1996, 2006). In the second type of scenario, the birth environment of the solar system was like the self-enriched massive SFRs of today (Jura et al. 2013), and the abundances of the radionuclides are the result of extensive averaging in the SFR. Some models are a mix of the two types (e.g., Gounelle & Meynet 2012). The two types of scenario are described in Section 2 and Section 3 below and their relative likelihoods are compared in Section 4. Section 5 describes implications for the nature of the SLR carriers.

2. CHANCE ENCOUNTERS

The chance encounter scenarios emphasize the discrete nature, or "granularity" (Wasserburg et al. 1996), of stellar nucleosynthesis events that could have seeded parental solar system material with nuclides. They can be described by an equation based on a geometric series summing individual nucleosynthesis events (encounters) with an average temporal spacing δt followed by a final actual free-decay time Δt (Wasserburg et al. 2006; Lugaro et al. 2014):

$$\frac{N_R}{N_S} = \left[\frac{P_R}{P_S} \frac{\delta t}{T} \left(1 + \frac{e^{-\delta t/\tau}}{1 - e^{-\delta t/\tau}} \right) \right] \exp(-\Delta t/\tau), \qquad (1)$$

where N_i and P_i are numbers and production rates for radionuclides (R) and stable isotope partners (S), respectively, T is the age of the Galaxy (7.4 Gyr at the time of solar system formation), Δt is in this case the time interval between the last event (LE) and the birth of the solar system, and τ is the mean life of R against radioactive decay. Dividing N_R by N_S eliminates the effects of element-specific chemistry when evaluating Equation (1) for different radionuclides. N_R/N_S ratios are well known for the early solar system from precise measurements of the radioactive decay products of the SLRs and the relative abundances of the longer-lived nuclides in meteoritic materials (Huss et al. 2009). Comparisons of different radionuclides are further facilitated by dividing the abundance ratio on the left-hand side of Equation (1) by the production ratio on the right-hand side. Production ratios are obtained from models of stellar nucleosynthesis (Rauscher et al. 2002; Woosley & Heger 2007). The resulting quotient, $(N_R/N_S)/(P_R/P_S)$, for different radionuclides depends on the radioactive mean lifetime τ, all else being equal. Therefore, if the radionuclides inherited by the solar system from its parent molecular cloud were all of similar average age, $(N_R/N_S)/(P_R/P_S)$ should vary only with τ, with the shorter-lived nuclides being less abundant relative to their production rates than the longer-lived nuclides. Equation (1) allows for differences in the ages of the nuclides depending upon the astrophysical environment in which they formed.
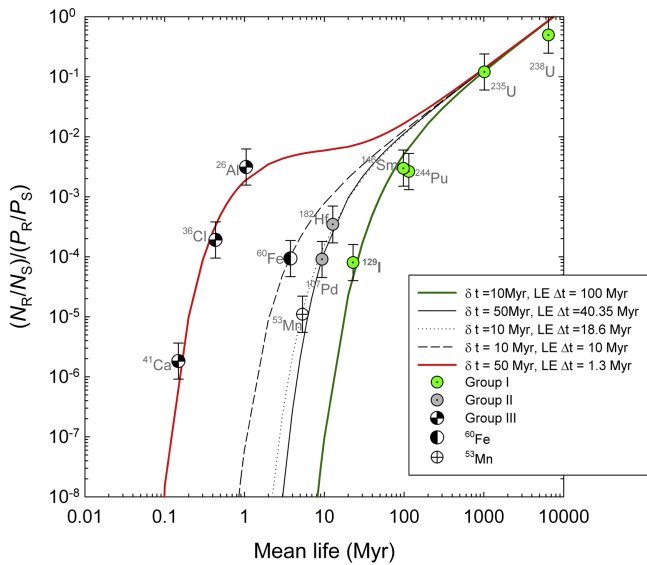
Figure 1. Plot of radionuclide abundances divided by those of their stable nuclide partners (N_R/N_S) and production ratios (P_R/P_S) vs. mean decay lifetime for radionuclides present at the birth of the solar system. The values for the abundance ratios, production ratios, and decay lifetimes are from published values (Young 2014) updated with new production ratios for ^{182}Hf and ^{107}Pd (Lugaro et al. 2014). Model curves are from Equation (1) fit to the different nuclide groups as indicated in the legend and in the text.

Equation (1) can be used to derive models of $\log[(N_R/N_S)/(P_R/P_S)]$ versus $\log(\tau)$, resulting in several groupings of radionuclides for which production ratios are well known (Figure 1, where radionuclides made primarily by spallation are omitted). These groupings succinctly summarize many of the relationships previously described in the literature (e.g., Wasserburg et al. 2006). For example, the relative concentrations of r- and (in one case) p-process products ^{129}I, ^{146}Sm, ^{244}Pu, ^{235}U, and ^{238}U are all explained by Equation (1) using $\delta t = 10$ Myr and $\Delta t = 100$ Myr (Figure 1). The value for δt is consistent with the frequency of supernova events affecting random positions in the Galactic disk (Meyer & Clayton 2000) and so is appropriate for these SNe-derived nuclides. Here we label these isotopes as Group I. Similarly, it was shown recently (Lugaro et al. 2014) that a single set of values for δt and Δt can explain the relative concentrations of both ^{107}Pd and ^{182}Hf, both nuclides being dominantly s-process products from AGB stars (Figure 1). A value for δt of 50 Myr, appropriate for encounters with AGB stars, and a similar value for Δt of 40.35 Myr fit the $\log[(N_R/N_S)/(P_R/P_S)]$ values for ^{107}Pd and ^{182}Hf (Figure 1). We refer to these radionuclides as Group II. ^{53}Mn and ^{60}Fe are treated separately from Groups I and II. ^{53}Mn is also fit by the Group II curve but its origin must be distinct as it is a SN product, suggesting a shorter δt interval. ^{60}Fe requires its own Δt (Figure 1). The shortest-lived nuclides, labeled Group III, have $\log[(N_R/N_S)/(P_R/P_S)]$ values that are explained with Equation (1) using $\delta t = 50$ Myr and $\Delta t = 1.3$ Myr (Figure 1). The latter model reflects the fact that these short-lived nuclides have no "memory" of events prior to their most recent synthesis. Five distinct models defined by five Δt values (δt values are prescribed a priori by astrophysical constraints) and represented by five curves are therefore required to explain the radionuclide abundances in Figure 1, one each for Groups I, II, and III and two others for ^{53}Mn and ^{60}Fe.

3. SELF-ENRICHMENT

The self-enrichment of SFRs features the enhanced effects of winds from Wolf–Rayet (WR) stars. WR stars have massive progenitors ($M_* > 20$–$25 \, M_\odot$). Their large progenitor masses ensure that they have short lifetimes (several million years) and are therefore spatially correlated with SFRs since they do not have time to flee their birth environment before they die (Young 2014). In one recent formulation of the self-enrichment scenario (Young 2014), all 12 radionuclides considered in Figure 1 are explained by a single model based on a two-phase interstellar medium (ISM) composed of a molecular cloud phase (MC) and a diffuse phase and with a molecular cloud mass fraction x_{MC} of ~0.17, equivalent to that today. The model equation (Jacobsen 2005, pp. 548–557; Young 2014) is

$$\log\left(\frac{N_{R,MC}}{N_{S,MC}}\right) - \log\left(\frac{P_R}{P_S}\right)$$
$$= 2\log\tau - \log[(1 - x_{MC})\tau_{MC} + \tau] - \log T, \quad (2)$$

where the abundances of radionuclides and their stable partners now refer to those in the molecular cloud phase and environs in the SFR ($N_{R,MC}$ and $N_{S,MC}$, respectively) as opposed to the diffuse ISM outside the SFR. The radionuclide production terms relevant to the molecular cloud setting are cast in terms of production from supernovae (P_R^{SNe}) and production from WR winds (P_R^W):

$$\frac{P_R}{P_S} = \frac{\Lambda_{SNe}P_R^{SNe}}{\Lambda_{SNe}P_S} + \frac{\Lambda_W P_R^W}{\Lambda_{SNe}P_S}, \quad (3)$$

where Λ_W and Λ_{SNe} are the relative efficiencies for trapping the two sources of nuclides in the SFR. WR production values are listed by Young (2014). The model fits the solar system data using two independent parameters: an enhancement of WR wind production over SN production in SFRs, with $\Lambda_W/\Lambda_{SNe} \sim 4000$, and a sequestration time of nuclides in molecular cloud dust, $\tau_{MC} \sim 200$ Myr (Figure 2). τ_{MC} is the *average* time spent in SFR molecular clouds before exiting by dispersal or by incorporation into stars. Because individual clouds exist for shorter time spans than the SFR as a whole (see the Appendix), time spent passing from one cloud to another via intercloud space in the SFR is included in the residence time. The radionuclide residence time τ_{MC} of ~200 Myr is consistent with the lifetime of dust in the ISM (Tielens 2005) and the timescale for converting molecular clouds to stars (Draine 2011). In general, large values for Λ_W/Λ_{SNe} are consistent with the fact that massive stars like WR progenitors apparently do not typically end their lives as energetic SNe but rather collapse by fallback to form black holes directly (Fryer 1999; Smartt 2009). In this way, the products of WR winds are enhanced relative to SNe products in SFRs sufficiently massive as to host a population of large stars (Young 2014). The fate of WR stars is debated, however, as evidenced by different interpretations of recent spectroscopic data for type IIb supernova 2013cu (Gal-Yam et al. 2014; Groh 2014), making a priori evaluation of Λ_W/Λ_{SNe} tenuous. Nevertheless, high values for Λ_W/Λ_{SNe} on an SFR scale are also favored by the fact that most supernovae derive from stars that outlive their association with their birth environs (Young 2014).
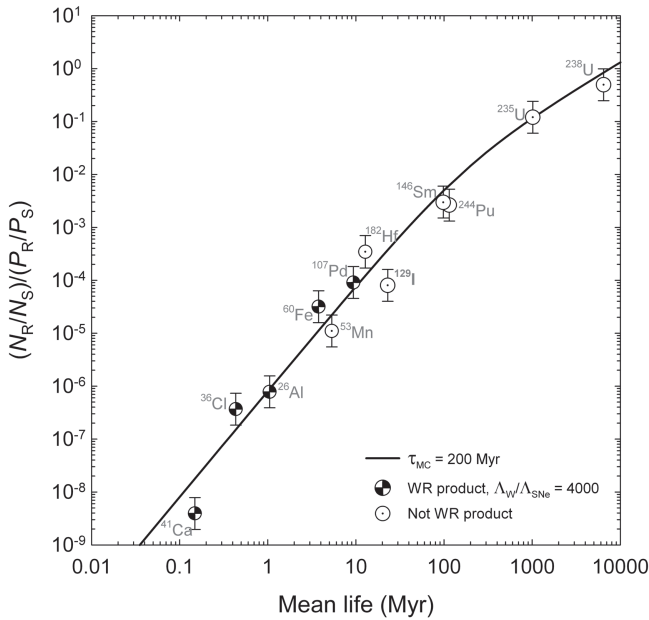
Figure 2. Plot of radionuclide abundances divided by those of their stable nuclide partners (N_R/N_S) and production ratios (P_R/P_S) vs. mean decay lifetime for radionuclides in the early solar system. The plot is similar to Figure 1 but with ordinate values calculated using production ratios that include $\Lambda_W/\Lambda_{SNe} = 4000$ and published WR production terms compiled by Young (2014). The curve is Equation (2) fit to the data using $\Lambda_W/\Lambda_{SNe} = 4000$ and $\tau_{MC} = 200$ Myr.

4. ASSESSING PROBABILITIES

In an effort to move beyond qualitative arguments for and against these disparate hypotheses, Bayes'/Laplace's theorem is used here to assess the relative likelihoods for the two classes of explanations exemplified by Figures 1 and 2. The relevant equation is (Jeffreys 1961; Schwarz 1978)

$$\frac{P(h_1|\boldsymbol{x})}{P(h_2|\boldsymbol{x})} = \underbrace{\frac{P(\boldsymbol{x}|\boldsymbol{\theta}_1 h_1)}{P(\boldsymbol{x}|\boldsymbol{\theta}_2 h_2)} N^{-(1/2)(n_{\theta,1}-n_{\theta,2})}}_{\text{Bayes Factor}} \overbrace{\frac{P(h_1)}{P(h_2)}}^{\text{Priors}}, \quad (4)$$

where $P(h_i|\boldsymbol{x})$ is the posterior probability of hypothesis h_i given data $\boldsymbol{x}$, $P(\boldsymbol{x}|\boldsymbol{\theta}_i h_i)$ is the conditional probability for data $\boldsymbol{x}$ assuming that hypothesis h_i represented by parameters $\boldsymbol{\theta}_i$ is correct, N is the number of data (in this case 12), $n_{\theta,i}$ are the numbers of parameters defining the models, and $P(h_i)$ are the a priori probabilities for hypotheses i independent of the data. The conditional probabilities are assessed as the integrals of the χ^2 probability densities for each fit. The models in Figure 1 together are defined by five independent parameters yielding seven degrees of freedom and a combined reduced χ^2 of 1.14, corresponding to $P(\boldsymbol{x}|\boldsymbol{\theta}_1 h_1) = 0.335$ (0.5 is optimal). The model in Figure 2 is defined by two independent parameters, 10 degrees of freedom, and a reduced χ^2 of 0.95, corresponding to $P(\boldsymbol{x}|\boldsymbol{\theta}_2 h_2) = 0.484$. Assuming equal priors of 0.5 each for now, Equation (4) leads to

$$\frac{P(h_1|\boldsymbol{x})}{P(h_2|\boldsymbol{x})} = \underbrace{\frac{0.335}{0.484} 12^{-(1/2)(5-2)}}_{\text{Bayes Factor}} \overbrace{\frac{0.5}{0.5}}^{\text{Priors}} = 0.017. \quad (5)$$

This ratio, being $\ll 1$, constitutes "strong" evidence (Kass & Raftery 1995) that the SFR hypothesis (h_2) is favored over the chance encounter hypothesis (h_1). The fits to the data are effectively equally good and cannot distinguish the models. Rather, the result in Equation (5) is attributable to the information criterion part of the Bayes factor (Schwarz 1978) that penalizes models for many versus fewer fit parameters; there is a quantifiable cost to probability when using more model parameters than necessary to fit the data (a quantification of Occam's razor).

Schwarz's formulation of the Bayesian information criterion (BIC) used as the Bayes factor in Equation (5) is one of two common methods for assessing the relative merits of complexity versus parsimony in model selection (Aho et al. 2014). The other is the Akaike information criterion (AIC, Aikaike 1973). The AIC excels at selecting models with the best predictive power at the risk of unwarranted complexity while the BIC excels at selecting the "correct" model where it is present among the models being evaluated (Kass & Raftery 1995; Aho et al. 2014). Because of their general nature, we assume that the two types of scenario being evaluated here encompass the correct model. In any event, application of the AIC to the analysis above gives a result similar to that in Equation (5); the probability ratio in Equation (5) is 0.05 using the AIC, similar to the BIC-derived value of 0.02.

The simple priors used in the analysis here are formally "noninformative" in so far as they imply no prior knowledge of the veracity of one hypothesis relative to the other. An inherent lack of a priori information about various aspects of the models under consideration leads to a preference for the simple priors used here. In principle, however, the conservative assumption of equal priors could be replaced by astrophysical constraints in the form of proper probability densities (Sivia & Skilling 2006). For example, the prior for the chance encounter scenario could include a distribution representing the chances that an average nucleosynthesis interval δt of 10 Myr would be followed by a significantly longer final delay Δt of 100 Myr (i.e., many σ from the mean interval represented by δt) as required by the data for ^{129}I, ^{146}Sm, ^{244}Pu, ^{235}U, and ^{238}U. Although perhaps not possible at present, a refined prior for the self-enrichment model could depend in part on an a priori probability distribution for Λ_W/Λ_{SNe}.

5. CARRIER GRAINS

If self-enrichment of an SFR is indeed the explanation for the solar abundances of the SLRs, the solar system abundances of these isotopes must be averages of progenitor dust grains with SLR abundances ranging from zero (old grains) to values greater than solar (very young grains). A model for the ^{26}Al/^{27}Al produced by random grain growth from large numbers of grains produced in an SFR is shown in Figure 3 following the procedures in Young (2014). Details are presented in the Appendix. The central limit theorem ensures that the ^{26}Al/^{27}Al distribution of the new grains is Gaussian even though the initial distribution is heavily skewed towards very low values due to decay for 10^8 yr (the residence time as ISM grains). Because of the central limit theorem, the self-enrichment scenario also indicates that even small variations in isotope ratios in solar system grains are echoes of larger (by orders of magnitude) dispersion in their molecular cloud precursors.
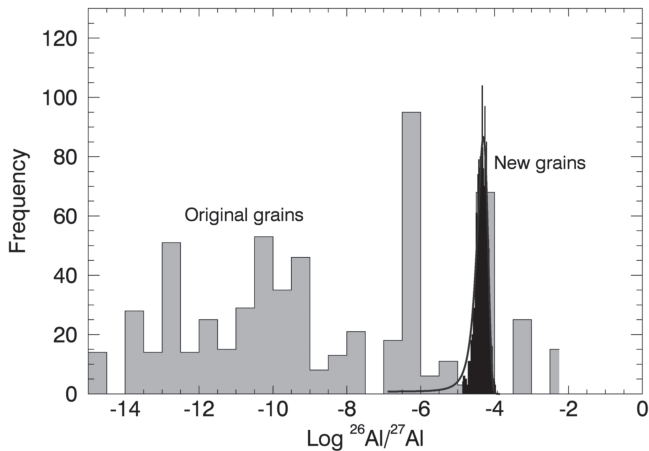
Figure 3. Results of a model for $^{26}Al/^{27}Al$ hosted by grains in an SFR (gray) sampled at random by grain growth (black). The resulting distribution of $^{26}Al/^{27}Al$ in the newly grown grains is Gaussian, a consequence of the central limit theorem. The solid curve shows the Gaussian fit to the new grain distribution (note the abscissa is on a log scale). The spread in original grain values over many orders of magnitude is erased by the grain growth.

For example, the peak in ISM grain sizes is at about 0.1 μm (Tielens 2005, p. 461) while hibonite grains in meteorites—among the most primitive solar system solids—are generally $\sim$30 μm in size. Assuming an ISM-like grain size in the star-forming clouds, it takes about 27 million cloud grains to make a single 30 μm hibonite grain (based on identical densities). The central limit theorem states that $\sigma' = \sigma(n)^{-1/2}$ where σ is the standard deviation of the original dust, σ' is the standard deviation of the newly grown grains, and n is the number of original grains averaged to make the newly grown grains. Accordingly, the predicted variability in $^{26}Al/^{27}Al$ for the molecular cloud precursors to solar system hibonites should be about 5000 times that exhibited by the hibonites. Where evidence for live ^{26}Al is evident in hibonite grains, the initial $^{26}Al/^{27}Al$ values are about $5 \times 10^{-5} \pm 1 \times 10^{-5}$ (Liu 2008), suggesting a range in the precursor grain values of $^{26}Al/^{27}Al$ of $\sim$0 to 0.05, not dissimilar to the large range in Figure 3. Similarly, it takes about 8000 hibonite grains to make the more evolved calcium–aluminum-rich inclusions (CAIs) with typical diameters of $\sim$300 μm. CAIs are among the most primitive objects in carbonaceous chondrite meteorites, but are generally acknowledged to post-date the hibonite grains (Liu 2008). The dispersion about the mean in CAI initial $^{26}Al/^{27}Al$ predicted from the spread in hibonite values is $\pm 0.01 \times 10^{-5}$, a value that is generally consistent with the tightly clustered CAI $^{26}Al/^{27}Al$ data (Jacobsen et al. 2008). A narrowing of the range in ^{50}Ti isotope anomalies of $\pm\sim$30‰ in hibonites to $\pm\sim$0.1‰ in CAIs is further evidence for averaging (Niederer et al. 1985; Ireland 1988; Chen et al. 2009). The reduction in dispersion from many orders of magnitude in original dust to a very narrow range of values in solar system grains is consistent with the averaging implied by the self-enrichment origin for ^{26}Al.

6. CONCLUSIONS

The inductive approach codified by the Bayes/Laplace theorem allows us to assess the relative likelihoods that the abundances of the radionuclides in the early solar system were the result of chance encounters with discrete stellar sources or instead the result of averaging over a large number of sources typical of massive SFRs. The analysis favors the latter. There

is, therefore, no compelling evidence that tracing a particular nuclide to one particular stellar source (e.g., proximal supernova) is the appropriate interpretation of the radionuclide data. Rather, the abundances of these nuclides are well explained if they were controlled by their mean lifetimes against radioactive decay and the characteristic steady-state residence time of material in SFRs prior to incorporation into stars. This result suggests that the solar system formed in a large SFR not unlike Cygnus today.

APPENDIX

Following the procedure described by Young (2014), an IDL+Fortran code was written to simulate the production of ^{26}Al in the vicinity of molecular cloud material for prolonged periods of time ($\sim$100 Myr). The goal is to track the availability of ^{26}Al to cloud material that survives multiple episodes of star formation that are spatially correlated on the kiloparsec scale for of the order of 10^8 years, as described by Elmegreen (2007) and Elmegreen & Hunter (2010).

Fictive star clusters were generated using the mass generation function of Kroupa et al. (1993) modified by Brasser et al. (2006). With this function, initial masses for each star j are drawn at random according to the expression

$$M_j/M_\odot = 0.01 + (0.19x^{1.55} + 0.05x^{0.6})/(1-x)^{0.58}, \quad (6)$$

where x is a random number uniformly distributed between 0 and 1. For the results in this paper 5000 stars per cluster (i.e., 5000 random draws for x) were used, representing the high end of cluster populations where WR stars (i.e., O stars) are most likely to be found. Clusters are born every 1.5 Myr in these simulations, consistent with the cluster frequency observed in the Cygnus SFR today (Comeron & Pasquali 2012). The cloud material is exposed to each of the local clusters simultaneously. In order to allow for a finite interval of star formation (i.e., all stars in a cluster are not born at exactly the same time), the birth date of each star in a cluster was altered at random over a total time interval of 1 Myr. The exact value of this blurring of birth dates turns out to have little effect on the models.

The minimum progenitor mass for WR activity is $\sim$20–25 $M_\odot$. The lifetimes of stars in this mass range mean that all WR stars eject winds in the vicinity of cloud material in this model. For 5000 stars per cluster, the average number of WR stars per cluster is 1.6 ± 1.2 (1σ, based on sampling 500 clusters) with a range generally between 1 and 5. A maximum size for progenitors to form collapse supernovae was set at 20 $M_\odot$ in the present calculations.

The mass of ^{26}Al ejected by WR winds and supernovae proximal to cloud material is tallied as a function of time. Integrated masses ejected by WR winds were obtained in approximate form from Gounelle & Meynet (2012). The total yields as a function of stellar progenitor masses used for interpolation for all masses are given in Table 1, where the maximum stellar mass considered was 120 $M_\odot$. Yields for supernovae were obtained from interpolation of values given
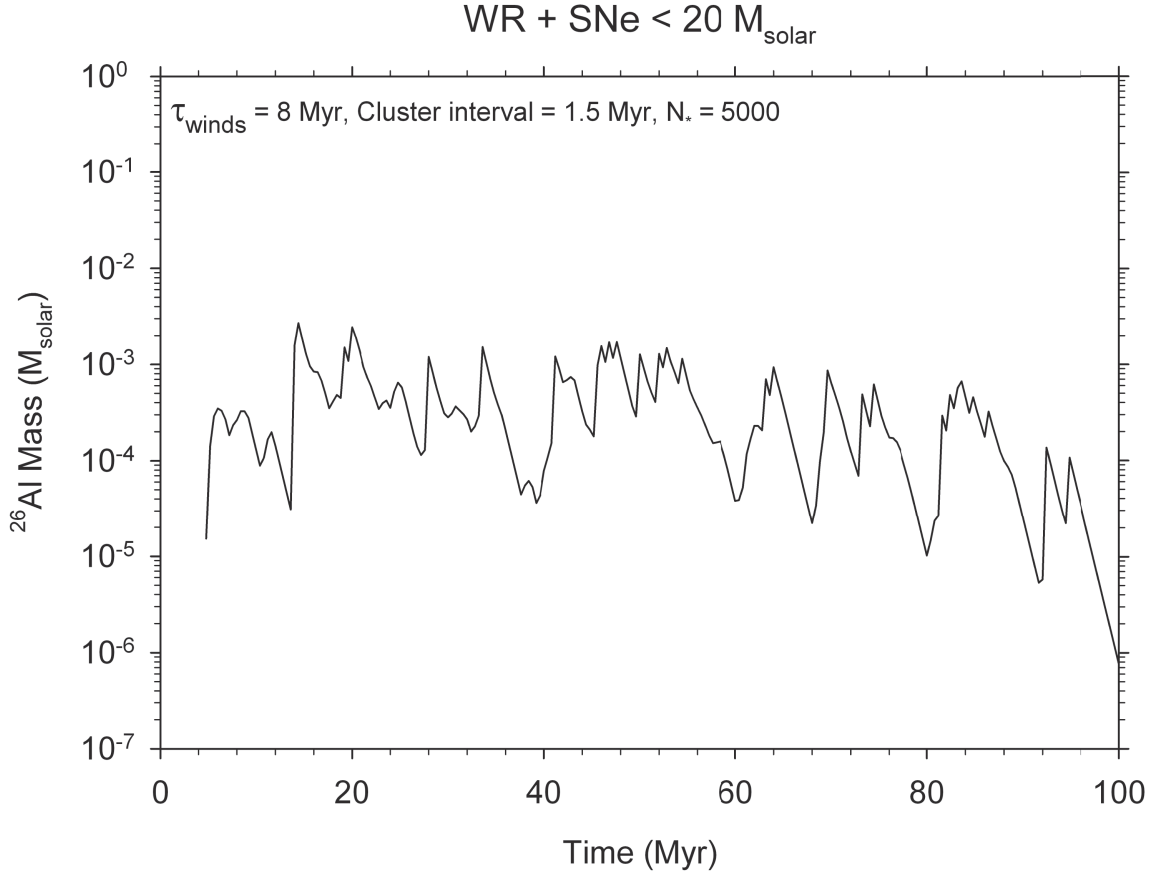
WR + SNe < 20 M$_{solar}$

τ_{winds} = 8 Myr, Cluster interval = 1.5 Myr, N$_*$ = 5000

Figure 4 Mass of ^{26}Al produced in the model described in this Appendix as a function of time in a long-lived SFR. Wolf–Rayet winds dominate production of ^{26}Al about 50% of the time in these calculations.

Table 1
Wolf-Rayet ^{26}Al Yields as a Function of Progenitor Mass Used for Interpolation

Progenitor Mass ($M_\odot$)	^{26}Al ($M_\odot$)
20	2.0×10^{-10}
25	2.0×10^{-6}
30	2.0×10^{-5}
60	7.0×10^{-5}
80	1.0×10^{-4}
120	2.0×10^{-4}

by Chieffi & Limongi (2013). Exact values for yields are not important to the conclusions to be drawn from this simulation.

For every time step each parcel of ^{26}Al delivered by a star that experiences winds or ends its life as a supernova within 10 Myr (the expected time for association of a star and its natal cloud) of the initiation of the cluster was added to the total inventory of available ^{26}Al for the duration of the model. For supernova ejecta a single pulse of ^{26}Al with mass $M_{^{26}\mathrm{Al},j}^{\mathrm{SNe}^o}$ is added to the total inventory of ^{26}Al at the moment the star explodes (if the star does so within 10 Myr of the birth of its cluster). The radioactive decay of this parcel of ^{26}Al from supernova j is followed through time t using

$$M_{^{26}\mathrm{Al},j} = M_{^{26}\mathrm{Al},j}^{\mathrm{SNe}^o} \exp(-t/\tau_{^{26}\mathrm{Al}}). \qquad (7)$$

Products of winds evolve in a more complicated fashion because they are delivered over extended periods of time, with time constant τ_{W}, simultaneous with radioactive decay with mean life $\tau_{^{26}\mathrm{Al}}$. Their evolution is therefore governed by the equation

$$\frac{dM_{^{26}\mathrm{Al},j}}{dt} = \frac{M_{^{26}\mathrm{Al},j}^{\mathrm{W}}}{\tau_{\mathrm{W}}} - \frac{M_{^{26}\mathrm{Al},j}}{\tau_{^{26}\mathrm{Al}}}, \qquad (8)$$

where $M_{^{26}\mathrm{Al},j}$ is the time-dependent mass of ^{26}Al evolving from stellar source j as modified by radioactive decay and $M_{^{26}\mathrm{Al},j}^{\mathrm{W}}$ is the evolving mass of ^{26}Al derived from stellar source j at time t. The solution for each WR source j is

$$M_{^{26}\mathrm{Al},j}(t) = \frac{\tau_{^{26}\mathrm{Al}}}{\tau_{\mathrm{W}} - \tau_{^{26}\mathrm{Al}}}$$
$$M_{^{26}\mathrm{Al}}^{\mathrm{W}^o}(\exp(-t/\tau_{\mathrm{W}}) - \exp(-t/\tau_{^{26}\mathrm{Al}})), \qquad (9)$$

where $M_{^{26}\mathrm{Al}}^{\mathrm{W}^o}$ is the total integrated mass of ^{26}Al delivered by winds from source j. Inspection of the time evolution of wind products given by Gounelle & Meynet (2012) suggests a value for τ_{W} of ~8 Myr. Many O stars end their lives prior to this time interval, so the time evolution in Equation (8) is cut short with the death of the WR star and is replaced by simple decay of the remaining ^{26}Al using the form of Equation (7). For purposes of comparison with real data, the mass of ^{27}Al inherited from the ISM in the model was set to yield the observed solar system ^{26}Al/^{27}Al for the average mass of ^{26}Al returned by the model. The result for the mass of ^{26}Al in the SFR with respect to time is shown in Figure 4.

Grain growth from the molecular cloud material was simulated by sampling and averaging the products of the evolution described above, taking into account radioactive decay of each parcel of ^{26}Al from the time each parcel was produced to the time of grain sampling. A grain sampling time of 100 Myr was used. The results are not affected by the exact timing of sampling. For example, if there are 500 bins composed of molecular cloud grains of 500 different ages, and each is sampled at random 100 aliquots at a time, and this is repeated 1000 times, the resulting distribution of 1000 newly formed grain populations is converted from a highly asymmetrical population skewed towards effectively zero ^{26}Al to a Gaussian distribution. The simulations of grain growth using this strategy are found to be in accordance with the central limit theorem such that

$$\sigma' = \sigma (n)^{-1/2}, \tag{10}$$

where σ' is the standard deviation for the new population of grains, σ is the standard deviation for the original population of smaller grains, and n is the number of smaller grains comprising the larger grains.

REFERENCES

Aho, K., Derryberry, D., & Peterson, T. 2014, Ecology, 95, 631
Aikaike, H. 1973, in Proc. Second Int. Symp. Information Theory: Akademiai Kaido, ed. B. N. Petrov & F. Csaki (Budapest, Hungary: Akademiai Kiado), 267
Brasser, R., Duncan, M., & Levison, H. 2006, Icar, 184, 59
Cameran, A. G. W., & Truran, J. W. 1977, Icar, 30, 447
Chen, H.-W., Lee, T., Lee, D.-C., & Iizuka, Y. 2009, Terrestrial Atmospheric, and Ocean Sciences, 20, 703
Chieffi, A., & Limongi, M. 2013, ApJ, 764, 36
Comeron, F., & Pasquali, A. 2012, A&A, 543, 23
Draine, B. T. 2011, Physics of the Interstellar and Intergalactic Medium (Princeton, NJ: Princeton Univ. Press)
Elmegreen, B. G. 2007, ApJ, 668, 1064
Elmegreen, B. G., & Hunter, D. A. 2010, ApJ, 712, 604
Fryer, C. L. 1999, ApJ, 522, 413
Gal-Yam, A., Arcavi, I., Ofek, E., et al. 2014, Natur, 509, 471
Gounelle, M., & Meynet, G. 2012, A&A, 545, A4
Groh, J. H. 2014, A&A, 572, L11
Huss, G., Meyer, B. S., Srinivasan, G., Goswami, J. N., & Sahijpal, S. 2009, GeCoA, 73, 4922
Ireland, T. R. 1988, GeCoA, 52, 2827
Jacobsen, B., Yin, Q.-z., Moynier, F., et al. 2008, E&PSL, 272, 353
Jacobsen, S. 2005, in Chondrites and the Protoplanetary Disk, ed. A. Krot, E. Scott, & B. Reipurth, Vol. 341 (San Francisco, CA: ASP)
Jeffreys, H. 1961, Theory of Probability (3rd ed.; Oxford: Clarendon)
Jura, M., Xu, S., & Young, E. D. 2013, ApJL, 775, L41
Kass, R. E., & Raftery, A. E. 1995, J. Am. Stat. Assoc., 90, 773
Kroupa, P., Tout, C. A., & Gilmore, G. 1993, MNRAS, 262, 545
Liu, M.-C. 2008, PhD thesis, Univ. California Los Angeles
Lugaro, M., Heger, A., Osrin, D., et al. 2014, Sci, 345, 650
Meyer, B. S., & Clayton, D. D. 2000, SSRv, 92, 133
Niederer, F. R., Papanastassiou, D., & Wasserburg, G. J. 1985, GeCoA, 49, 835
Rauscher, T., Heger, A., Hoffman, R., & Woosley, S. 2002, ApJ, 576, 323
Schwarz, G. 1978, AnSta, 6, 461
Sivia, D. S., & Skilling, J. 2006, Data Analysis: A Bayesian Tutorial (2nd ed.; Oxford: Oxford Univ. Press)
Smartt, S. J. 2009, ARA&A, 47, 63
Tielens, A. 2005, The Physics and Chemistry of the Interstellar Medium (Cambridge: Cambridge Univ. Press), doi:10.1017/CBO9780511819056
Wasserburg, G. J., Busso, M., & Gallino, R. 1996, ApJL, 466, L109
Wasserburg, G. J., Busso, M., Gallino, R., & Nollett, K. M. 2006, NuPhA, 777, 5
Woosley, S., & Heger, A. 2007, PhR, 442, 269
Young, E. D. 2014, E&PSL, 392, 16